Structural characterization of *Argania spinosa* Moroccan wooden artifacts during natural degradation progress using infrared spectroscopy (ATR-FTIR) and X-Ray diffraction (XRD)

Abdellatif Boukir [a,*], Somia Fellak [a], Pierre Doumenq [b]

[a] *Laboratory of Applied Chemistry, Faculty of Sciences and Technology of Fez, Sidi Mohamed Ben Abdellah University, B.P. 2202, Imouzzer Road, Fez, Morocco*
[b] *Laboratory of Environmental Chemistry, UMR CNRS 7376, MPO Team, Aix-Marseille University, Europôle Arbois BP 80, 13545Aix in Provence Cedex 04, France*

A B S T R A C T

The present work is focused on spectroscopic study of four samples of Argan wooden artifact pertaining to the 17th, 18th, 20th and 21st centuries. The objective is to characterize their unknown structures by the study of their non degraded parts and to investigate changes occurred in their degraded parts due to the natural degradation process. Attenuated total reflectance Fourier transform infrared spectroscopy gauges the presence of many functional groups related to cellulose I and/or II (OH, C–O–C and –CH$_2$), hemicelluloses (particularly C=O acetoxy ester band at 1732 cm^{-1}), and lignin (OH phenolic, C$_{ar}$-O and C=C$_{ar}$) and provides qualitative information on the state of wood alteration by informing on the evolution of new former C=O bands. The degree of conversion to carbonyl group, especially quinone or *p*-quinone at 1650 cm^{-1}, is correlated to lignin degradation, while the absence of the C=O acetoxy absorption is ascribable to occurred deterioration in hemicelluloses, and partial degradation of cellulose with enhancement of the C=O region between 1730-1630 cm^{-1}. X-ray diffraction determines the presence of two forms of cellulose; amorphous cellulose at 18.5° 2θ and predominant crystalline cellulose I_β at $2\theta = 22.6°$ which characterized by an intense peak. The decrease of crystallinity index values confirms the deterioration level and obvious changes in crystallinity level. However, the microcrystalline structure appears unaltered because no significant changes were observed for calculated cristallite seize. The obtained results depend on the prolonged time of ageing, natural deterioration phenomena, and wood part (internal or external) that is exposed to degradation. The combination of these two methods is useful for an accurate estimation of the degradation level of argan wood.

1. Introduction

Extending from southwest to southeast Morocco, the argan tree (*Argania spinosa* L. Skeels) represents an endemic natural outgrowth which covers about 950, 000 ha. It constitutes the third most common wood specie in Morocco, behind the thuya (*Tetraclinis articulata*) and evergreen oak (*Quercus ilex*). It benefits local populations economically because of the argan oil extracted from almonds largely used as antioxidants in food (Khallouki et al., 2015), and cosmetic products (Charrouf and Guillaume, 2014). The extracted fruit of the argan tree is known for its potential pharmaceutical applications, while its leaves are used to isolate pectin polysaccharides (Hachem et al., 2016). On the other hand, argan wood has been mostly used in the artisanal sector as a source of art works and craft timber, as well as material for house building and domestic fire.

Today, the deterioration process of this cultural material is underway and the progress of conservation work encounters many difficulties which are often invasive, impeding the interpretation of the work or changing its appearance and aesthetics. To overcome the preservation problematic, it would be fundamental to probe the structural aspects of the altered wood polymers.

The primary polymers that constitute argan wood are: cellulose, hemicelluloses, and lignin. The cellulose consists of monomer units of *β*-D-glucose and cross-linked between the molecular chains with a large number of hydrogen bonds that could be converted into the formation of both amorphous (less ordered) and crystalline (highly ordered) structure. The hemicelluloses are known to be more stable for hydrolyzed reactions. Compared to cellulose, the hemicelluloses are constituted by poly-

* Corresponding author.
E-mail address: aboukir@gmail.com (A. Boukir).

saccharides rings without any crystalline forms (Peng et al., 2015). The lignin represents an amorphous polymer with two and/or three substituted-phenol ring (monomer) including methoxy and hydroxyl groups or methoxy, hydroxyl and allyl groups. The aromatic monomers chromophore contents are syringyl, sinapyl, and guaiacyl (coniferyl alcohhol) (Tamburini et al., 2015).

The photolability of the inner chromophoric groups underlies the vulnerability of lignocellulosic fibers. The main factors that are responsible for the deterioration are: the absorption of light with 80–95% UV absorptions (case of lignin fraction), aerobic conditions, chemical oxidants and physical factors as temperature (Fellak and Boukir, 2018). In addition, wood can be easily degraded by the fungus attack and the lignin degradation products are known to be highly inhibitory to cellulases (Mithra and Padmaja, 2017). All these factors result in significant modifications of chemical, physical and mechanical properties of lignocellulosic fibers changing, consequently, the color of the structure chain correlated to the nature of wood species and regenerated chromophores (Peng et al., 2015), and leading to the loss of archaeological materials (Fellak and Boukir, 2018).

Previous non-destructive tools have been applied on archaeological wood and lignocellulosic fibers to elucidate the group functionalities, chemical bonds and chemical changes in order to monitor their deterioration level (Delmotte et al., 2008; Fellak and Boukir, 2018). Among the most used methods, we find the ATR-FTIR (Attenuated Total Reflectance Fourier Transform Infrared) spectroscopy and XRD (X-ray diffraction).

ATR-FTIR spectroscopy was widely used to investigate and monitor many types of art works in cultural heritage and building materials such as reinforced with polypropylene (Peng et al., 2015), cellulosic wood weathering degradation (Lionetto et al., 2012), and construction materials and their chromatic alteration (case of cathedral of S. Giorgio in Italy) (Barone et al., 2008). In a recent study, it is used to monitor and to confirm the reinforced methacrylate/halloysite nanoclay wood polymer nanocomposites, expected to be used in building materials in exterior or interior applications (Rahman et al., 2017).

For XRD analysis, cristallinity index Cr.I value was determined by using Segal method (Segal et al., 1959) in order to study crystallinity behaviors. The combined Cr.I data of XRD and FTIR techniques revealed an increase in the crystallinity index of the weathering wood (Lionetto et al., 2012). Whereas, in a recent study on degraded cellulose in ancient historical documents (Hajji et al., 2015a), it is reported that Cr.I values decrease with extended time of degradation and influenced by environmental conditions. The decrease in Cr.I could be explained by the partial involvement of the crystalline phase in the alteration of the cellulose leading to a depolymerization in the microstructure and evolving towards an amorphous phase, and thus contributes by synergistic effect to the overall increase in the amorphous content. This finding might be correlated to the loss of glycosidic molecules in the crystalline content, conferring to the cellulose a low amount of molecular hydrogen bonds, and giving arise to a non-compact structure easily altered, correlated mainly to extended time of natural weathering degradation effects. The consolidated samples treatment was monitored by X-ray diffraction patterns.

In a recent study, the examination of experimental amorphous fractions of cellulose I_β at (18° 2θ intensity) and cellulose II materials at (16° 2θ intensity) with simulating the X-ray diffraction patterns of semi-crystalline cotton celluloses, as well as the study of the effect of cristal size on the Segal crystallinity Index (Cr.I) values have been reported (Nam et al., 2016). The change in crystallinity degree was influenced by various conditions such as mercerization, temperature and treatment time. Thus, the exploitation of the Segal method must consider the degree of polymorphic conversion that affects the diffraction pattern.

No published works have been reported on the structural characterization and study of historical argan wood exposed to natural degradation process, especially by the combination of non-destructive techniques. Therefore, the main goal of this research is to perform analyses to prove a clear picture of argan wooden artifact samples (degraded and non-degraded surfaces) belonging to the 17th, 18th, 20th and 21st centuries, in order to better define their functional groups, chemical constituents, structural elucidation and introduced changes which are related to their ages and to the nature of surface exposed to natural weathering process.

To achieve these purposes, two non-destructive methods have been applied: ATR-FTIR spectroscopy for qualitative analyses and in order to provide information about the presence of functional groups and other specific structural features and X-ray diffraction for the study of chemical and microfibrils crystallinity changes.

2. Materials and methods

2.1. Sampling

The present study is conducted on degraded and non-degraded parts of four wooden materials pertaining to the 17th, 18th, 20th and 21st centuries originated from Agadir region (southwest of Morocco). Degraded wood samples were taken from the surface of pieces and compared with non-degraded samples which were cut from 4 cm below the surface of the wood piece. This comparison aims at evaluating the effect of natural degradation process. It is worth to note that the samples were dated by specialist researchers using radiocarbon dating method. Thus, the dimensions of wood samples are $200 \times 200 \times 100$ mm^3 (tangential $\times$ radial $\times$ longitudinal directions). The eight characterized samples are listed in Table 1.

2.2. ATR-FTIR spectroscopy

Fourier's transformed infrared (FTIR) transmission spectra was carried out through a BRUCKER VERTEX 70® spectrometer coupled to a Hyperion® microscope. All samples were scanned using Platinum diamond ATR (Attenuated Total Reflectance) in the wavenumber region between 4000 and 400 cm^{-1} with a resolution of 4 cm^{-1}. At each position 16 scans were averaged. The room temperature and humidity were controlled during analysis.

2.3. X-ray diffraction measurement

The X-ray diffraction (XRD) analysis was performed using an X'Pert Pro diffractometer operating with monochromatic Cu Kα radiation ($\lambda =$ 1.5406 Å), generated at a current of 30 mA and a voltage of 40 kV. The scattering angle of 2θ was detected from 10° to 70° using a step size of 0.016° with 40s exposure at each step. The crystallinity study was based on the determination of two parameters:

- Cr.I (%) crystallinity index that was described by Segal method (Segal et al., 1959), using the following equation:

$$Cr.I \ (\%) = \left(\frac{I_{002} - I_{am}}{I_{002}} \right) \times 100 \tag{1}$$

Where I_{002} is the diffraction peak intensity corresponding to the (002) lattice plane at 2θ–22° and I_{am} is the diffraction intensity at 2θ–18°

Table 1
Wood sample descriptions.

Sample	Description of analyzed part	Age (Century)
A	non degraded	21st
A'	Degraded	
B	non degraded	20th
B'	Degraded	
C	non degraded	18th
C'	Degraded	
D	non degraded	17th
D'	Degraded	

corresponding to the amorphous background.

The average size of crystallite that was calculated from the Scherrer equation based on the width of the diffraction patterns. In this work, crystalline size was calculated from the 002 lattice plane of microcrystalline cellulose (MCC) samples.

$$D_{(hkl)} = K \, \lambda_1/H \cos\theta \qquad (2)$$

where $D_{(hkl)}$ is crystalline size (nm), K is Scherrer constant (0.89), λ_1 is X-ray wavelength (1.5406 Å), H is the full width at half maximum (FWHM) in radians and θ the corresponding Bragg angle.

3. Results and discussion

3.1. ATR-FTIR spectroscopy

FTIR spectroscopy, as a useful technique to study wood, has been applied in order to identify the chemical and molecular structure of cellulose, hemicelluloses, and lignin as components constitute the studied wood samples as well as the changes produced on their structures through natural ageing.

3.1.1. Characterization of non-degraded wood samples

In the first approach, we are interested in characterizing the argan wood samples by the analysis of non degraded part (samples A, B, C and D). The FTIR recorded spectra are displayed in Fig. 1. The assignment of bands detected by examination of ATR-FTIR spectra are summarized in Table 2.

As illustrated in the table above, the main bands associated to the cellulose and hemicelluloses contents were detected at 3340, 3278, 3240, 2890, 1732, 1462, 1425, 1375, 1318, 1163, 1112, 1034 and 898 cm^{-1}, while lignin component was characterized by the bands at 1595, 1505, 1268 and 1230 cm^{-1} and 834 cm^{-1}.

Fig. 1 shows the detection of broad absorption between 3750-3000 cm^{-1} that was attributed to the vOH stretching vibration of bonded hydroxyl groups in crystalline cellulose as well as in hemicelluloses and lignin (Laysandra et al., 2017; Zghari et al., 2018). The slight peak around 3278 cm^{-1} originating from v(O6 H6···O3) intermolecular hydrogen bonds (Schwanninger et al., 2004) in monoclinic cellulose I_β was observed (Schwanninger et al., 2004). However, it is still absent in an IR spectrum of triclinic I_α cellulose (Sanjay et al., 2018). This finding was confirmed by our XRD study (see the following XRD part). Usually, the large and broad absorption of O–H out of plane bending vibration arises between 750-700 cm^{-1}.
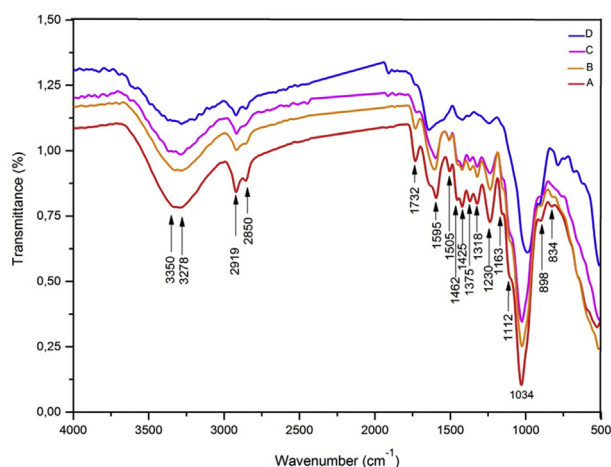

Fig. 1. FTIR spectra of non-degraded samples of argan wood (A: sample dating to 21st, B: sample dating to 20th, C: sample dating to 18th and D: sample dating to 17th century).

Table 2

Main ATR-FTIR bands in argan wood (degraded and non-degraded samples).

Wavenumber (cm^{-1})	Band assignments
3750–3000	v(OH) hydroxyl groups in lignin (phenolic + CH$_2$OH), cellulose and hemicelluloses Intermolecular hydrogen-bonded H–O–H stretching
3278	O6 H6···O3 intermolecular hydrogen bond (Zhicheng et al., 2015; Popescu et al., 2016) in cellulose I_β (Sassi et al., 2000; Schwanninger et al., 2004; Watanabe et al., 2006; Popescu et al., 2010; Peng et al., 2015; Santos et al., 2015; Ling et al., 2019; Boukir et al., 2019)
3240	I_α O6 H6···O3 intermolecular hydrogen bond (Schwanninger et al., 2004; Zhicheng et al., 2015; Popescu et al., 2016) in cellulose I_α (Sugiyama et al., 1991; Schwanninger et al., 2004; Popescu et al., 2011a; Santos et al., 2015; Ling et al., 2019; Boukir et al., 2019)
3000–2850	v$_{as}$CH$_2$ and v$_s$CH$_2$ in methylene and v$_{as}$CH$_3$, v$_s$CH$_3$ in methyl groups
1732	vC = O ester in acetoxy groups (H$_3$C-(C=O)–O-) in hemicelluloses
1650	vC = O in quinone or p-quinone
1595, 1505	vC = C$_{ar}$ skeletal vibration in phenolic ring (lignin motif type guaiacyl ie coniferyl with C-H$_{ar}$ out of plane deformation at 834 and 900-870 cm^{-1})
1462	δCH$_2$ asymmetric bending (scissoring) strong in cellulose I δCH$_3$ asymmetric bending in lignin (CH$_3$–O) and hemicelluloses (CH$_3$-(C=O)-)
1425	δCH$_2$ symmetric bending in crystallized cellulose I (strong) and amorphous cellulose (weak and shift to 1420 cm^{-1} in cellulose II and amorphous cellulose)
1375	δC-H and δ$_s$CH$_3$ in cellulose and hemicelluloses
1318	δCH$_2$ in crystallized cellulose I (wagging)
1268	vC$_{ar}$-O guaiacyl aromatic methoxyl group in lignin and cellulose (Zhicheng et al., 2015)
1230	vC$_{ar}$-O syringyl nuclei in lignin and hemicellulose (Zhicheng et al., 2015)
1163	C–O–C asymmetric stretch vibration in cellulose and hemicelluloses
1112	CH stretching vibrations in different groups of lignin and cellulose and hemicelluloses
1034	C–O–C skeletal vibration of polysaccharides ring
898	vC$_1$-O-C β-(1–4)-glycosidic linkage (weak and broad in cellulose I, strong and sharp in cellulose II)
834	γC-H$_{ar}$ (2C-H$_{ar}$ adjacent) out of plane bending of 1,2,4-tetra-substituted aromatic in lignin, with contribution of the band at 900-870 cm^{-1} (collapsed with vC$_1$-O-C β-(1–4)-glycosidic linkage)

The bands detected between 3000-2850 cm^{-1} were assigned to (sp^3) C–H stretching vibration at 2919 cm^{-1} (vCH$_3$, v$_{as}$CH$_2$), 2850 cm^{-1} (v$_s$CH$_2$) in methyl and methylene groups (Zghari et al., 2017). Asymmetric and symmetric bending vibration δCH$_3$ and δCH$_2$ scissoring in lignin (H$_3$C–O–Ar) and in hemicelluloses (H$_3$C-(C=O)–O-) are expected at 1465 cm^{-1} (δ$_{as}$CH$_3$, δ$_{as}$CH$_2$) and 1375 cm^{-1} (δ$_s$CH$_3$), respectively (Boukir et al., 1998a,b; Colom et al., 2003). Comparing this result with other research findings, the δCH$_2$ in lignin and carbohydrates arose between 1450 and 1400 cm^{-1} (Guiliano et al., 2000). The scissoring strong peak at 1430 cm^{-1} was attributed to the cellulose I, while cellulose II and amorphous cellulose were characterized by weak peak detected at 1420 cm^{-1} (Song et al., 2015). On the other hand, the bands at 1425 and 1375 assigned to CH$_2$ and CH$_3$ bending vibration, respectively, characterize the mixture of both crystalline and amorphous cellulose (Huang et al., 2012).

The detection of bands at 1318 and 1163 cm^{-1} that attributed to δCH$_2$ and C–O–C asymmetric stretch vibration respectively was a proof of the presence of crystallized I cellulose (Colom et al., 2003). Usually in amorphous cellulose, these bands were located at 1336 and 1156 cm^{-1} respectively (Lionetto et al., 2012). Nevertheless, there are no clear indications of their presence in our FTIR spectra (Fig. 1) suggesting that the microcrystalline structure of non-degraded sample wasn't seriously

affected by natural degradation process.

In FTIR spectra (Fig. 1), the C=O ester band at 1732 cm^{-1} was found in all four samples (A, B, C, D) decreasing in intensities from recent to aged one, and ascribed to acetoxy group (H$_3$C-(C=O)–O-). It corresponds to the free conjugated carbonyl groups of carboxylic acid originating from oxidative primary alcohol CH$_2$OH on side chain of xylan in hemicelluloses or in heterocyclic cellulosic ring (Rahman et al., 2017).

The absorption intensities at 1595 and 1505 cm^{-1} corresponded to C=C$_{ar}$ aromatic skeletal vibration over the lignin syringyl-guaiacyl matrix (Zghari et al., 2017). The strong band at 1595 cm^{-1} is correlated to the polar aromatic compound containing the phenolic group (Boukir et al., 1998a,b) with consistent features confirming the presence of lignin (Zghari et al., 2018). It can overlap with water band usually expected between 1620 cm^{-1} and 1640 cm^{-1} (Hajji et al. 2015a, 2016; Peng et al., 2015). Furthermore, lignin polymer was also characterized by the arising of C$_{ar}$-O band detected at 1230 cm^{-1} which is due to coupled OH bending and C–O stretches vibrations (Boukir et al., 1998a,b). Thus, to distinguish the presence of syringyl motif (1,2,3,5-tetrasubstituted aromatic) and/or guaiacyl ie coniferyl motif (1,2,4-trisubstituted aromatic) alcohols in lignin argan wood, the fingerprinting region <1000 cm^{-1} was exploited. The absence of the C-H$_{ar}$ band at 866 cm^{-1} related to one isolated C-H$_{ar}$ can rule out the presence of syringyl motif in lignin and confirmed the presence of guaiacyl (1,2,4-trisubstituted aromatic) motif by the detected band at 834 cm^{-1} characteristic of γC-H$_{ar}$ with contribution of the γC-H$_{ar}$ peak at 900-870 cm^{-1} (collapses with vC$_1$-O-C β-(1–4)-glycosidic linkage in cellulose) (Boukir et al., 1998a,b).

It is widely held that the range between 1200 and 900 cm^{-1} covers the complex C–O and C–C stretching, anti-symmetric bridge C–O–C as well as CCH and OCH deformation vibrations. In all samples spectra, the band at 1112 cm^{-1} is indicative of CH, CO deformation or stretching vibrations in different groups of lignin and carbohydrates (Hajji et al., 2016).

In the fingerprint region of cellulose and hemicelluloses between 1170-950 cm^{-1}, the largest and intense absorption bands centered at 1034 cm^{-1} were assigned to vC–O stretching of polysaccharides (Poletto et al., 2011; Gurgel et al., 2012; Falcão et al., 2014).

The broad absorption band with a weak pointed shoulder at 898 cm^{-1} ascribed to the stretching vibration of C$_1$–O–C of β-(1–4)-glycosidic linkages in cellulose I and amorphous fraction, and corroborates with recent literatures data (Abidi et al., 2014; Hajji et al., 2015a, 2016; Acharya et al., 2017); however, this band is subject to many controversies (Sun et al., 2004; Schwanninger et al., 2004; Song et al., 2015; Hajji et al., 2015a; Zghari et al., 2018). According to Sun et al., (2004); the studied band corresponded to the CH$_2$ rocking vibration of cellulosic material and/or to glycosidic C$_1$–H deformation with ring vibration contribution, while Schwanninger et al. (2004) have attributed it to the anomeric C-groups, or C$_1$–H deformation and/or ring valence vibration. As for Song et al. (2015) and Zghari et al., (2018); they have referred it to the C$_1$–O–C stretching vibration of β-(1–4)-glycosidic linkage which is weak and broad for cellulose I, and strong and sharp for cellulose II and amorphous cellulose. In addition, Manzato et al. (2017) have assigned it to the glycosidic C–H rocking vibration characteristic of the cellulose structure material.

During the extended time of deterioration (18th and 17th centuries), a manifested decrease in both the weak pointed shoulder peak and glycosidic C$_1$–O–C band (Fig. 2: C, C', D, D') highlighted the occurred changes by altering the linkage C$_1$–O–C β-(1–4)-sugar of the polymeric cellulose fractions and forcing the rearrangement in the hydrogen bond network (changing crystalline to amorphous fraction) (Proniewicz et al., 2001; Hajji et al., 2015a, 2016; Zghari et al., 2018). The presence of the new rearrangement is responsible for the decreasing intensities of the unresolved bands in the region of 1480–1300 cm^{-1} (Fig. 2: C' and D') assigned generally to the in-plane bending vibrations of H–C (H-CC, H-CO, H-OC, H–C–H), justifying the produced change from crystalline to amorphous content, while the decrease in the intensities of H–C might be correlated to the oxidation of primary alcohol (H$_2$–COH) to aldehyde
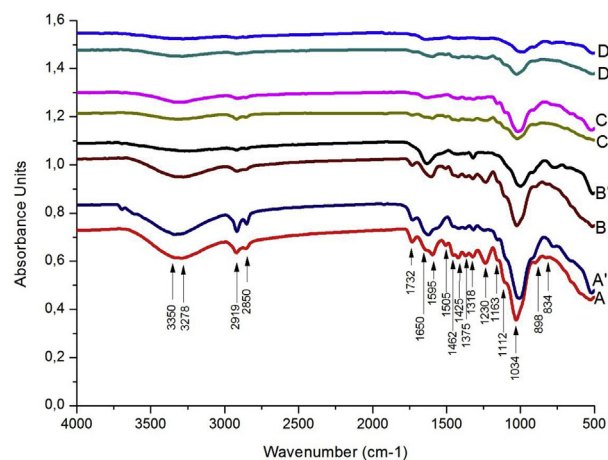

Fig. 2. FTIR spectra of superposed degraded samples (A': sample dating to 21st, B': sample dating to 20th, C': sample dating to 18th and D': sample dating to 17th century) and non-degraded samples of argan wood (A: sample dating to 21st, B: sample dating to 20th, C: sample dating to 18th and D: sample dating to 17th century).

carbonyl group of which in turn oxidizes towards a carboxylic acid, and/or secondary alcohol (H–CH–OH) towards a ketone former.

The FTIR finding of degraded samples (C' and D') corroborates well with XRD results by decreasing in the crystallinity index from youngest A' (Cr.I = 49%) to very oldest one D' (Cr.I = 25%) (*see* section 3.2). Additionally, this absorption band was used to quantify the cellulose I fraction with a ratio of (A$_{1430}$/A$_{900}$) in the cellulose structure sensitive to the both absorptions at 1430 and 900 cm^{-1} (Abidi et al., 2014; Acharya et al., 2017).

3.1.2. Study the effect of natural degradation on lignocellulosic constituents

In the second approach, we focused on the study of the effect of natural degradation of A', B', C' and D' argan wood samples dating from the 21st, 20th, 18th and 17th centuries, respectively, by comparing their profiles with each of the non-degraded ones. The main spectral changes are illustrated in Fig. 2.

A drastic change has been shown in spectrum of 3650–3100 cm^{-1} for all degraded samples (Fig. 2 A', B', C' and D') with decreasing in band's intensities during prolonged exposure to natural weathering passing from un-aged sample dating from the 21st century to the aged one dating from 17th century. The disappearance of these bands in most aged samples dating from the 17th century (Fig. 2D') can be explained by the sample undergoing oxidation phenomena. In the spectra of youngest samples dating from the 21st and 20th centuries, the detection of the band between 3568-3577 cm^{-1} assigned to intra-molecular hydrogen bond in phenolic group of lignin may suggest the presence of residual lignin (Schwanninger et al., 2004; Stark and Matuana, 2004).

For all wood samples, there is appreciable dropping in the spectrum between 3600-2500 cm^{-1} characteristic of OH acidic and/or hydrogen bonded related to enol forms in tautomeric equilibrium that appears more pronounced in spectra of youngest samples especially the sample dating from the 21st century (Fig. 2 A and A'). However, the disappearance of this band in oldest samples dating from the 17th century reveals an advanced oxidation of alcohols groups.

The interesting proportion of oxidized spectrum at 3000-2850 cm^{-1} related to methylene and methyne groups (–CH$_2$–OH, –CH–OH), undergoes a net decrease passing from un-aged sample to aged one. In our study, we note the absence of the C–H absorption between 2850-2720 cm^{-1} confirming the oxidation of C=O aldehydic. Consequently, we can suggest that the advanced alteration of cellulose component results from the conversion of the C=O aldehydic to C=O carboxylic acid.

The same trend was observed for CH$_2$ and CH sensitive bending at 1462-1300 cm^{-1} except the peak at 1318 cm^{-1} in spectrum of sample A'

(21st century) and B' (20th century). The persistence of this band is subject to prominent changes in the crystalline fraction of cellulose (Delmotte et al., 2008; Zghari et al., 2018). For the latest, the δCH_2 in-plane deformation gains in intensity and informs on the occurred modification in cellulose structure. The increase of its intensity accompanied by the disappearance of the band located at 1337 cm^{-1} indicates clearly the presence of the crystallized cellulose form with the absence of amorphous fraction. We can suggest the involvement of the amorphous fraction by promoting the formation of the new and large crystals. The obtained data are in total accordance with several FTIR literature studies (Hajji et al., 2015a). Our FTIR results match perfectly with the crystallinity study (calculated Cr.I % index values) described in the following section (X-ray diffraction).

A total disappearance of the band at 1732 cm^{-1} with a drastic damage has been noticed in the spectra of sample dating from the 20th, 18th and 17th centuries respectively (Fig. 2 A', B' and C'). Thus, an hydrolysis reaction on the ester functionality has likely occurred resulting in the formation of alcohol sugar followed by oxidative degradation of heterocyclic sugar with both opening chain and arising of a new C=O bands of ketone, aldehyde or carboxylic acid groups. In all non-degraded samples, it decreased from the youngest to the oldest samples relative to exposure time to natural degradation processes.

In our FTIR spectra, the C=O quinonic band was detected at 1650 cm^{-1} in all degraded samples (Fig. 2 A', B', C' and D') with large and intense absorption (Müller et al., 2003), indicating well the occurred oxidation of lignin fraction. The FTIR examination of C=O (1800-1550 cm^{-1}) photo-oxidized from polar phenol with using deconvolution routines and FTIR oxidation index allowed easy determination of this absorption as a quinone or aromatic alkyl ketone Ar–CO–R at 1695 cm^{-1}, as well as diconjugated carbonyl groups which indicates diarylketone Ar–CO–Ar or p-quinone at 1660 cm^{-1} (Guiliano et al., 2000; Boukir et al., 2001). The enhancement of this band was explained mechanistically by the cleavage of the C–O alkyl bond branched directly to aromatic ring

(C–O–Ar or H$_3$C–O–Ar bond) (Müller et al., 2003).

Generally, the increase of the principal C=O spectral region between 1710-1550 cm^{-1} is an indication of the lignin degradation level resulting from many oxidation mechanism aspects. Overall, several difficulties were encountered to assess the regeneration of oxidized C=O groups in the region 1710-1550 cm^{-1}, due especially to the interference with different type of polar broad band's, such as: carbonyl C=O absorptions (1710-1640 cm^{-1}), enol tautomer equilibrium forms towards ketone or aldehyde forms (1680-1540 cm^{-1}), aromatic phenolic bands (C=C$_{ar}$: 1620-1550 cm^{-1}) (Boukir et al., 1998a,b; Boukir et al., 2001), as well as δOH (1640-1620 cm^{-1}) in plane bending vibration of adsorbed water in lignin (Hajji et al., 2015a, 2016).

The both aromatic skeletal lignin vibrations and their functional groups absorption are subject of many changes and might be justified by the influence of environmental conditions such as temperature, UV. According to Huang et al. (1995) and Müller et al. (2003), the cleavage of the β-O-4 bond gives arise to the excited phenoxy aromatic radical, which in turn converted to the formation of quinone chromophore after further oxidative reactions, and so, the proposed oxidative mechanism of lignin was described in detail (Scheme 1). While in recent studies, Lu et al. (2016) reported a new model of cleavage mechanism for 2-phenoxy-1--phenylethanol lignin pattern over palladium catalysts, explaining the formation of both oxidative structures: quinone and acetophenone forms.

In our FTIR spectra, the quinone chromophore former could be combined to the formation of diconjugated carbonyl groups resulted an increase of the carbonyl absorption bands at 1650 cm^{-1}, accompanied by the loss of the intensities of aromatic skeletal vibration at 1505 and 1595 cm^{-1}, justifying well the occurred deterioration of the aromatic lignin structures.

In cellulose and hemicelluloses contents, the both hemiketal function of anomeric carbon ring and alcohol functions (secondary and primary) of glycosidic ring are subject to degradation process by oxidative reactions of primary alcohols groups in side chain, or by chain opening
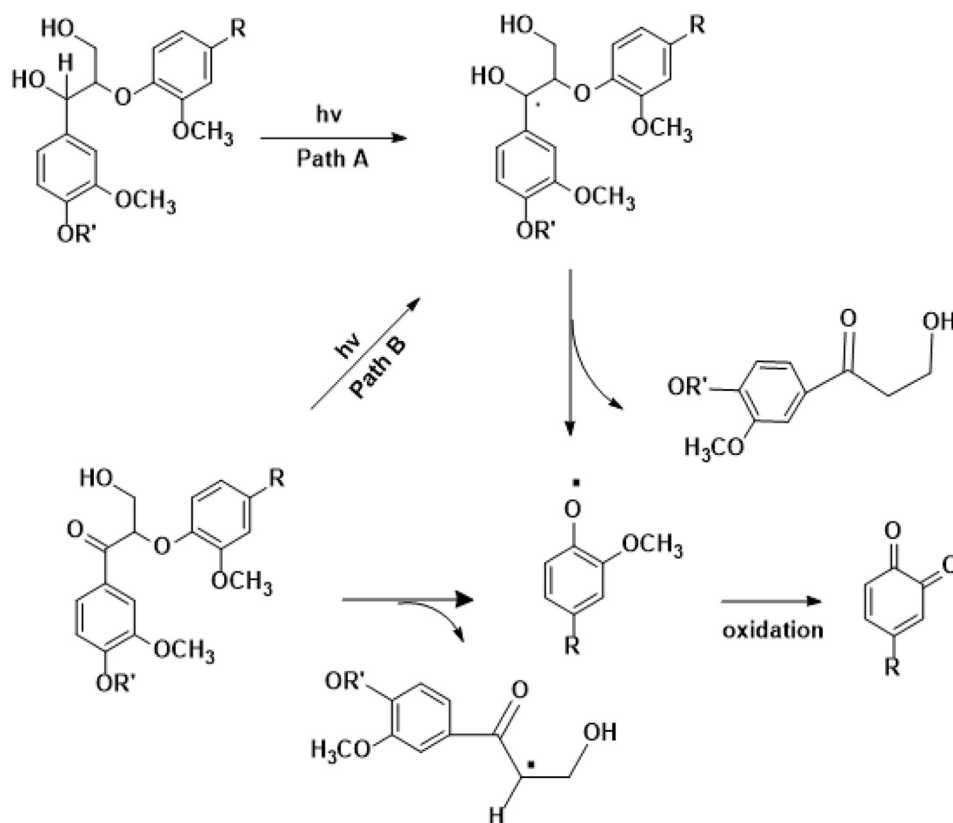
Scheme 1. Formation of quinone structure as a result of the cleavage of the β-O-4 bond according to Müller et al. (2003) and *cited references*.

(cycle alteration) of adjacent secondary alcohols groups of glycosidic ring, followed by their oxidation towards the formation of carbonyl groups, thus, justifying the presence of the advanced oxidative reaction.

The cleavage occurred on the β-1,4-glycosidic bond allowed to the formation of hydroxyl groups, which in turn the alcohols are oxidized to C=O groups (ketone or aldehyde to carboxylic acid). Thus, a noticeable increase in the region of 1710–1600 cm^{-1} provides information about the degree of damage and cellulose degradation due to the regression in the intense and large fingerprint region (1200-900 cm^{-1}) of cellulose. The considerable decrease of the majority bands intensities in this region has been observed for all samples (Fig. 2).

The identification of degraded lignin was based on characteristics band vibrations exposed to deterioration phenomenon: C$_{ar}$-O large polar centered at 1230 cm^{-1}, C=C$_{ar}$ at 1595 cm^{-1} large polar band with the contribution of the band at 1505 cm^{-1} and C-H$_{ar}$ at 3100-3000 cm^{-1} stretching and below to 1000 cm^{-1} out of plane bending. Due to this complexity, the C$_{ar}$-O has been chosen to monitor the degradation process.

The most affected sample was the one dating from the 17th century (Fig. 2D') suggesting the occurrence of both degradation in cellulose-hemicelluloses and lignin with respect to the reduction in typical C$_{ar}$-O and C=C$_{ar}$ lignin absorptions at 1230 cm^{-1} and 1595 cm^{-1} respectively. This phenomenon is much less pronounced or absent in the most recent wood samples dating from the 21st century (Fig. 2A').

The large polar lignin derived-peak (C$_{ar}$-O) centered at 1230 cm^{-1} considerably lost its intensity with exposure time and is absent in all degraded samples dating from the 18th and 17th centuries (Fig. 2 C' and D'). The evolution of this absorption band (C$_{ar}$-O) towards conjugate C=O stretching vibration at lower frequency of C=O (1700-1650 cm^{-1}) reveals the altered phenolic ring (Boukir et al., 1998a,b) resulting the lignin deterioration. This phenomenon may be explained by conversion of the methoxy substituents (dealkylation) on aromatic ring and on side chains to hydroxyl groups more exposed to oxidation reactions. The secondary reactions on side chain (hydroxy-allyl) of guaiacyl alcohol units lead to the conversion into guaiacyl-aldehyde (Müller et al., 2003; Tamburini et al., 2015).

The examined profiles of FTIR spectra of degraded and non-degraded samples show that the abundant fraction corresponds more to cellulose and hemicelluloses. They are the most influenced polymers by degradation phenomenon and therefore appeared to be less stable than lignin.

3.2. X-ray diffraction analysis

X-ray diffraction has been used in order to study the crystallinity behaviors of cellulose in argan wood. The XRD spectra of degraded and non-degraded samples have been reported in Figs. 3 and 4 respectively. The Cr.I crystallinity index and crystallite seize values (D_{002}) were calculated in order to evaluate the crystallinity behaviors of cellulose in studied samples. The obtained results are presented in Tables 3 and 4, respectively.

The X-ray diffractograms of the non-degraded samples (Fig. 3 A, B, C and D) showed the same profiles with two large humps accompanied by the lower peak at 34.52° 2θ. The intense peaks arose at 22.6° 2θ (Fig. 3), whereas the profiles of degraded samples present some differences (Fig. 4).

The qualitative evaluation of X-ray diffractograms of all wood samples shows the same diffraction features of crystalline cellulose as the dominant phase. Generally, the practical XRD range was from 5° to 50° 2θ and centered at 35° 2θ. It covers the significant band intensities that are representatives of both crystalline and amorphous cellulose components. Hence, hemicelluloses and lignin do not display any diffraction peaks but diffuse scattering halos in the 2θ range from 12° to 27° 2θ, which overlap with the crystalline diffraction peak positions (Temiz et al., 2005; Nam et al., 2016).

In the diffractogram of degraded and non-degraded samples (Figs. 3 and 4), crystalline cellulose I_β has been determined by the presence of
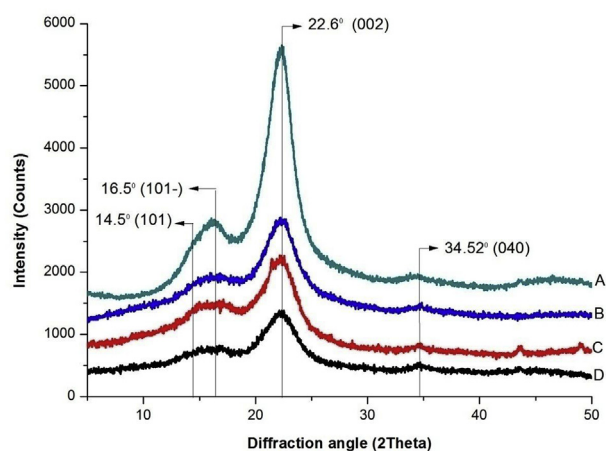
Fig. 3. XRD diffractogram of non-degraded samples of argan wood (A: sample dating from the 21st, B: sample dating from the 20th, C: sample dating from the 18th and D: sample dating from the 17th century).
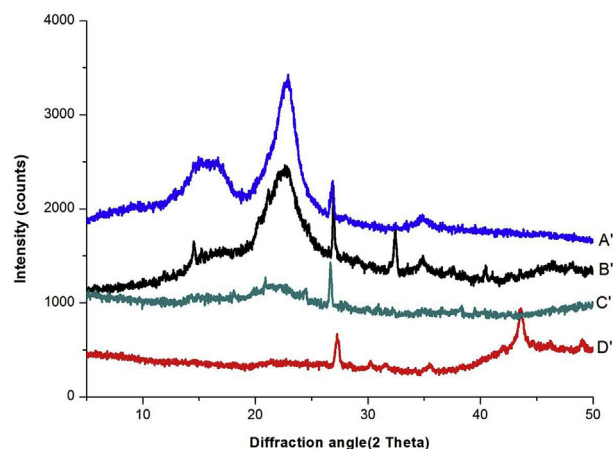
Fig. 4. XRD diffractogram of degraded samples of argan wood (A': sample dating from the 21st, B': sample dating from the 20th, C': sample dating from the 18th and D': sample dating from the 17th century).

Table 3
Crystallinity index of non-degraded and degraded samples of argan wood.

Samples		Cr.I (%)
Age (century)	Symbol	
21st	A	49
	A'	49
20th	B	43
	B'	48
18th	C	42
	C'	36
17th	D	32
	D'	25

four major peaks at 14.5°, 16.5°, 22.6° and 34.52° 2θ, which were ascribed to (101), (10$\bar{1}$), (002) and (040) crystallographic planes, respectively (Nam et al., 2016). For amorphous phase, diffracted profile was described at 18.5° (Segal et al., 1959; Hajji et al., 2015a; b; Hajji et al., 2016).

The XRD analysis permits the determination of crystalline cellulose phase. For all samples, the changes occurred and were evaluated by decreasing in crystallinity index Cr.I % from youngest to aged ones affecting the crystalline peak intensities in both degraded and non-degraded parts (48–25% and 43 to 32%, respectively), except the

Table 4

Crystallite seizes values of non-degraded and degraded samples of argan wood.

Samples		D_{002} (nm)
Age (century)	Symbol	
21st	A	0.174
	A'	0.043
20th	B	0.057
	B'	0.040
18th	C	0.044
	C'	0.036
17th	D	0.039
	D'	-

sample dating from the 20th century. So, the effect of degradation was less evident on microcrystalline structure for this sample.

In order to explain the XRD prominent outlier crystallinity index finding (Cr.I: 43%–48%) from B to B' samples (20th century), the confrontation of the latest data to FTIR results was necessary, allowing us to justify the Cr.I increasing value in B' (48%).

To support the XRD unexpected results, the FTIR data were exploited. The occurred change in IR profile spectra from B to B' (Fig. 2) and the decline in their polar and non-polar signal intensities in the regions of O–H (3700-3150 cm^{-1}), C–O–C (1160-850 cm^{-1}), H–C stretching vibrations (3000-2850 cm^{-1}), H-CC and H–CO bending vibrations of cellulose (1500-1310 cm^{-1}), as well as the disappearance of the resolved cellulose area bands (1480-1330 cm^{-1}) and more particularly the scissoring cellulose crystallinities bands at 1425 (cellulose I) and 1375 cm^{-1} (Colom et al., 2003; Schwanninger et al., 2004; Abidi et al., 2014; Hajji et al., 2015a, 2016; Acharya et al., 2017) towards a strong and broad unresolved cellulose absorption signal (1480-1330 cm^{-1}) ascribed to the presence of a mixture of crystalline and amorphous content (Invernizi et al., 2016; Zghari et al., 2018). The accompanied increase in the intensity of the rocking crystalline band of cellulose II at 1318 cm^{-1} (Evans et al., 1995; Abidi et al., 2014; Hajji et al., 2015b; Acharya et al., 2017; Zghari et al., 2018) also called wagging band (Manzato et al., 2017) confirms well the unaltered crystalline cellulose II undergoing regeneration and enhancement in its content and could overlap with the band at 1325 cm^{-1}, which might explains the occurred change in both amorphous and crystalline forms from B to B', and imputes the formation of a new crystalline forms in degraded sample B' (unresolved range: 1480-1335 cm^{-1}). This finding is supported by both XRD analyses with increase in Cr.I data from B (43%) to B' (48%). In addition, the enhancement in the area of oxidative IR C=O characteristic bands of sample B' (1750-1650 cm^{-1}) reports and justifies the partial occurred deterioration in the cellulose structure, less affected in the case of B than B'.

The combined results of XRD and FTIR analysis, corroborates well and promotes the regeneration and formation of a new crystalline domains and forms of cellulose fibers involving the amorphous phase more than the crystalline form. The reduction of the total amount of amorphous cellulose can also increases the relative Cr.I value.

Concerning the partial deterioration, it might be correlated mostly to the involvement of the amorphous part of cellulose, and probably accompanied by a minor contribution of the crystalline cellulose form of B' towards a different crystalline domains.

From the XRD results, the peak intensities (Figs. 3 and 4) and crystallinity index Cr.I % values (Tables 3 and 4) decreased gradually from youngest sample dating from the 21st century (A and A': 49%) to oldest one dating from the 17th century (32% for sample D and 25% for sample D') and from the non-degraded parts to degraded ones, confirming the deterioration level.

The decreasing values of XRD crystallinity index confirms the deterioration level and changes in microfibrils crystallinity passing from youngest samples to aged ones. The obtained results depend on the prolonged time of ageing, nature of deterioration phenomena, and of exposed part to deterioration process.

It is worth mentioning that all characterized samples present a low value (<50%) of Cr.I (%) parameter, presumably revealing that they suffered, to a large extent, from a natural degradation process. Another explanation is that our wood samples were more sensitive to degradation phenomena because they have a fragile and less dense structure. The noticeable decrease of this portion in D' degraded sample dating from the 17th century (Fig. 4), was confirmed by the absence of the sharp diffraction peak at 22.6° 2θ.

As shown in Table 3, the measured crystallinity index values decrease proportionally with age of sample even for the non-degraded sample in the following order A > B > C > D (Table 3), or for degraded sample in the following sequence A' > B' > C' > D' (Table 4). For each wood material, this parameter lowers its value during exposed time to natural degradation process, except the sample dating from the 20th century which allowed the increase of Cr.I % value from non-degraded part (Cr.I = 43%) to degraded one (Cr.I = 48%). Based on this unexpected result, it is suggested that for some oldest wood sample, the crystalline structure cannot be destroyed, because decreasing elasticity due to temperature increase causes a lack of sheer stress which destroys the hydrogen bonding of the crystalline structure (Shimur et al., 2014), and/or the degraded cellulose part was capable to form a new crystalline portion. This observation is confirmed by the increase of crystalline peak intensity at 22.6° 2θ for the (002) crystallographic plan as shown in Fig. 4B'. Our obtained cristallinity index Cr.I % values are in total concordance with the FTIR results (FTIR section before).

For un-aged sample dating from the 21st century (Fig. 3A and Fig. 4A'), no considerable changes in degraded and non-degraded parts were observed regarding the peak intensities, particularly for the intense peak at 22.6° 2θ; the samples present the same Cr.I value (49%). The result could be explained by the non-crystal structure alteration due to the recent and strongly built cellulose with associate hydrogen bond presenting resistance to degradation and destroying phenomena. In addition, we can suggest that the partial cellulose degradation was responsible for the regeneration of native crystalline and enrichment of the relative crystalline content in wood sample.

Mostly, the crystalline cellulose structure is related to the hydrogen bonding between intermolecular hydroxyl groups and included water (Barnette et al., 2012). Consequently, the loss of crystallinity is considered to result from opening of monosaccharides rings and destruction of their ordered packing (Kim et al., 2000; Li et al., 2011). The obtained data are in accordance with our FTIR results (see FTIR results section before), suggesting that the rapid evaporation of water caused limits to the chain mobility of cellulose, and consequently, its alignment, which decreases the crystallinity level. On the other hand, the quantification of cellulose crystallinity can be greatly influenced by the presence of other amorphous fraction as lignin and hemicelluloses and the decrease of crystalline mass fraction is directly correlated with reduction in crystallite size parameter.

The calculated value of crystallite seize linked to the 002 lattice plane reflection adopted for native cellulose I for all wood samples varies significantly depending on the age and nature (degraded or non-degraded part) of analyzed sample. The higher crystallite seize (0.174 nm) was observed for the non-degraded sample (A) dating from the 21st century, while 0.036 nm presents the lowest value that checked for the degraded sample (C') dating from the 18th century. The crystallite seize value of degraded sample dating from the 17th (sample D) century could not be calculated in contrast to the non-degraded one (sample D') that presents a value of 0.039 nm. This can be justified by the total deterioration of crystalline microfibrils and/or the presence of an important amount of amorphous fractions in wooden materials as lignin, hemicelluloses and extractives parts. The advanced age of this sample and its exposure to the natural degradation process for a long time was also another important cause for the enhanced deformation of its microcrystalline structure.

It has to be underlined that the amorphous cellulose is more susceptible to the alteration than crystalline cellulose, since it is more

accessible to water, microorganisms, etc. In fact, the mechanism of cellulose degradation, as hydrolysis, proceeds through a depolymerisation step, involving the amorphous regions of cellulose, until the size of oligomers becomes sufficiently small to allow metabolisation by microorganisms or solubilisation by water. According to the literature, the apparent lateral crystallite size, degree of crystallinity, the proportion of crystallite interior chains and cellulose fraction tend to decrease with decreasing of the wood density (Popescu et al., 2011b).

4. Conclusion

This work elucidates the structural characterization of degraded and non-degraded sample of four Moroccan argan woods by combining two analytical tools: ATR-FTIR spectroscopy and XRD.

The ATR-FTIR results show a significant decrease of all oxidizing regions spectrum bands originating from cellulose, hemicelluloses, and lignin proportionately with age of sample and degradation level. The lignin deterioration was evaluated by destruction or regression of aromatic ring bands and appearance of $\nu C = O$ quinone bands related to the oxidation phenomena of penolic groups, accompanied by the noticeable decrease in the intensities of $\nu C = C_{ar}$ and C_{ar}-OH bands. Furthermore, FTIR data revealed the presence of crystalline cellulose and damage caused by degradation on this fraction.

The XRD results permit the determination of crystalline cellulose phase. For degraded samples, the change occurred and was evaluated by decreasing in both crystallinity index Cr.I % and crystalline peak intensities; exception makes for the sample dating from the 20th century when the increase of Cr.I % be explained by the regeneration of native crystalline and enrichment of the relative crystalline content. So, the effect of degradation was less evident on microcrystalline structure for this sample. On the contrary, no change of crystallinity index has been shown in recent samples. The XRD crystallinity index results harmonize well with those obtained from FTIR data.

The obtained experimental results and adopted techniques provide the first information on structural characterization and degradation changes of argan wood; they constitute a background for the expertise in the field of wood art works. It can be applied in the topics of conservation and restoration science especially for wooden artifacts.

Declarations

Author contribution statement

Abdellatif Boukir & Somia Fellak: Conceived and designed the experiments; Performed the experiments; Analyzed and interpreted the data; Contributed reagents, materials, analysis tools or data; Wrote the paper.

Pierre DOUMENQ: Contributed reagents, materials, analysis tools or data.

Funding statement

This work was supported by the Department of Chemistry, Faculty of Science and Techniques of Fez, Sidi Mohammed Ben Abdellah University, Morocco.

Competing interest statement

The authors declare no conflict of interest.

Additional information

No additional information is available for this paper.

References

Abidi, N., Cabrales, L., Haigler, C.H., 2014. Changes in the cell wall and cellulose content of developing cotton fibers investigated by FTIR spectroscopy. Carbohydr. Polym. 100, 9–16.

Acharya, S., Hu, Y., Moussa, H., Abidi, N., 2017. Preparation and characterization of transparent cellulose films using an improved cellulose dissolution process. J. Appl. Polym. Sci. 134 (21), 44871.

Barnette, A.L., Lee, C., Bradley, L.C., Schreiner, E.P., Park, Y.B., Shin, H., Cosgrove, D.J., Park, S., Kim, S.H., 2012. Quantification of crystalline cellulose in lignocellulosic biomass using sum frequency generation (SFG) vibration spectroscopy and comparison with other analytical methods. Carbohydr. Polym. 89, 802–809.

Barone, G., La Russa, M.F., Giudice, A.L., Mazzoleni, P., Pezzino, A., 2008. The Cathedral of S. Giorgio in Ragusa Ibla (Italy): characterization of construction materials and their chromatic alteration. Environ. Geol. 55, 499–504.

Boukir, A., Guiliano, M., Asia, L., Mille, G., 1998a. A fraction to fraction study of photooxidation of BAL 150 crude oil asphaltenes. Analusis 26, 358–364.

Boukir, A., Guiliano, M., Doumenq, P., Mille, G., 1998b. Caractérisation Structurale d'asphaltènes pétroliers par spectroscopie infrarouge (FTIR). Application à la photooxidation. Comptes Rendus Chimie, Paris; t.1, série II. C., pp. 597–602.

Boukir, A., Aries, E., Guiliano, M., Asia, L., Doumenq, P., Mille, G., 2001. Subfractionation, characterization and photooxidation of crude oil resins. Chemosphere 43, 279–286.

Boukir, A., Mehyaoui, I., Fellak, S., Asia, L., Doumenq, P., 2019. The effect of the natural degradation process on cellulose structure of Moroccan hardwood fiber: a survey on spectroscopy and structural properties. Mediterr. J. Chem. 8 (3), 179–190.

Charrouf, Z., Guillaume, D., 2014. Argan oil, the 3S-years-of-research product. Eur. J. Lipid Sci. Technol. 116, 1316–1321.

Colom, X., Carrillo, F., Nogue, F., Garriga, P., 2003. Structural analysis of photodegraded wood by means of FTIR spectroscopy. Polym. Degrad. Stab. 80, 543–549.

Delmotte, L., Ganne-Chedeville, C., Leban, J.M., Pizzi, A., Pichelin, F., 2008. CP-MAS 13C NMR and FT-IR investigation of the degradation reactions of polymer constituents in wood welding. Polym. Degrad. Stab. 93, 406–412.

Evans, R., Newman, R.H., Roick, U.C., Suckling, I.D., Wallis, A.F.A., 1995. Changes in cellulose crystallinity during kraft pulping. Comparison of infrared, X-ray diffraction and solid state NMR results. Holzforschung 49, 498–504.

Falcão, L., Eduarda, M., Araújo, M., 2014. Application of ATR-FTIR spectroscopy to the analysis of tannins in historic leathers: the case study of the upholstery from the 19th century Portuguese Royal Train Lina Falcão. Vib. Spectrosc. 74, 98–103.

Fellak, S., Boukir, A., 2018. Moroccan Cedar softwood study: application of FT-Raman spectroscopy. MATEC Web Conf. 191, 00014.

Guiliano, M., Boukir, A., Doumenq, P., Crampon, C., Badens, E., Charbit, G., Mille, G., 2000. Supercritical fluid extraction of bal 150 crude. Oil Asphaltenes. Energ. Fuel. 14, 89–94.

Gurgel, L.V.A., Marabezi, K., Ramos, L.A., Curvelo, A.A.S., 2012. Characterization of depolymerized residues from extremely low acid hydrolysis (ELA) of sugarcane bagasse cellulose: effects of degree of polymerization, crystallinity and crystallite size on thermal decomposition. Ind. Crops Prod. 36, 560–571.

Hachem, K., Benabdesslem, Y., Ghomari, S., Hasnaoui, O., Kaid-Harche, M., 2016. Partial structural characterization of pectin cell wall from Argania spinosa leaves. Heliyon 2 (2), e00076.

Hajji, L., Boukir, A., Assouik, J., Kerbal, A., Kajjout, M., Doumenq, P., De Carvalho, M.L., 2015a. Multi-analytical approach for the evaluation of the efficiency of the conservation-restoration treatment of Moroccan historical manuscripts dating from the 16th, 17th and 18th centuries. Appl. Spectrosc. 69, 920–938.

Hajji, L., Boukir, A., Assouik, J., De Carvalho, M.L., Lakhiari, H., Kerbal, A., Doumenq, P., Mille, G., 2015b. Conservation of Moroccan manuscript papers aged 150, 200 and 800 Years. Analysis by infrared spectroscopy (ATR-FTIR), X-ray diffraction (XRD), and scanning electron microscopy energy dispersive spectrometry (SEM-EDS). Spectrochim. Acta, Part A 136, 1038–1046.

Hajji, L., Boukir, A., Assouik, J., Pessanha, S., Figueirinhas, J.L., De Carvalho, M.L., 2016. Artificial ageing paper to assess long term effects of conservative treatment. Monitoring by Infrared spectroscopy (ATR-FTIR), X-ray diffraction (XRD) and Energy dispersive X-ray fluorescence (EDXRF). Microchem. J. 124, 646–656.

Huang, Y., Pagé, D., Wayner, D.D.M., Mulder, P., 1995. Radical Induced Degradation og lignin model compound. Decomposition of one phenol-2-phenoxyethanol. Can. J. Chem. 73, 2079–2085.

Huang, X., Kocaefe, D., Kocaefe, Y., Boluk, Y., Pichette, A., 2012. Study of the degradation behavior of heat-treated jack pine (Pinus banksiana) under artificial sunlight irradiation. Polym. Degrad. Stab. 97, 1197–1214.

Invernizi, C., Daveri, A., Rovetta, T., Vagnin, M., Licchelli, M., 2016. Multi-analytical non-invasive approach to violin materials: the case of Antonio Stradivari "Hellier" (1679). Microchem. J. 124, 743–750.

Khallouki, F., Haubner, R., Ricarte, I., Erben, G., Klika, K., Ulrich, C.M., Owen, R.W., 2015. Identification of polyphenolic compounds in the flesh of Argan (Morocco) fruits. Food Chem. 179, 191–198.

Kim, U.J., Kuga, S., Wada, M., Okano, T., Kondo, T., 2000. Periodate oxidation of crystalline cellulose. Biomacromolecules 1, 488–492.

Laysandra, L., Kartika Sari, M.W.M., Soetaredjo, F.E., Foe, K., Putro, J.N., Kurniawan, A., Ju, Y., Ismadji, S., 2017. Adsorption and photocatalytic performance of bentonite-titanium dioxide composites for methylene blue and rhodamine B decoloration. Heliyon 3 (12), e00488.

Li, H., Wub, B., Changdao, M., Wei, L., 2011. Concomitant degradation in periodate oxidation of carboxymethyl cellulose. Carbohydr. Polym. 84, 881–886.

Ling, Z., Wang, T., Makarem, M., Santiago Cintrón, M., Nam, S., Edwards, J.V., Kim, S.H., Xu, F., French, A.D., 2019. Effects of ball milling on the structure of cotton cellulose. Cellulose 26, 305–328.

Lionetto, F., Sole, R.D., Cannoletta, D., Vasapollo, G., Maffezzoli, A., 2012. Monitoring wood degradation during weathering by cellulose crystallinity. Materials 5, 1910–1922.

Lu, J., Wang, M., Zhang, X., Heyden, A., Wang, F., 2016. β-O-4 bond cleavage mechanism for lignin model compounds over Pd catalysts identified by combination of first-principles calculations and experiments. ACS Catal. 6, 5589–5598.

Manzato, L., Rabelo, L.C.A., de Souza, S.M., da Silva, C.G., Sanches, E.A., Rabelo, D., Mariuba, L.A.M., Simonsen, J., 2017. New approach for extraction of cellulose from tucuma's endocarp and its structural characterization. J. Mol. Struct. 1143, 229–234.

Mithra, M.G., Padmaja, G., 2017. Strategies for enzyme saving during saccharification of pretreated lignocellulo-starch biomass: effect of enzyme dosage and detoxification chemicals. Heliyon 3 (8), e00384.

Müller, U., Rätzsch, M., Schwanninger, M., Steiner, M., Zobl, H., 2003. Yellowing and IR-changes of spruce wood as result of UV-irradiation. J. Photochem. Photobiol., B 69, 97–105.

Nam, S., French, A.D., Condon, B.D., Concha, M., 2016. Segal crystallinity index revisited by the simulation of X-ray diffraction patterns of cotton cellulose Iβ and cellulose II. Carbohydr. Res. 135, 1–9.

Peng, Y., Liu, R., Cao, J., 2015. Characterization of surface chemistry and crystallization behavior of polypropylene composites reinforced with wood flour, cellulose, and lignin during accelerated weathering. Appl. Surf. Sci. 332, 253–259.

Poletto, M., Pistor, V., Zeni, M., Zattera, A.J., 2011. Crystalline properties and decomposition kinetics of cellulose fibers in wood pulp obtained by two pulping processes. Polym. Degrad. Stab. 96, 679–685.

Popescu, C.M., Popescu, M.C., Vasile, C., 2010. Structural changes in biodegraded lime wood. Carbohydr. Polym. 79, 362–372.

Popescu, C.M., Popescu, M.C., Vasile, C., 2011a. Structural analysis of photodegraded lime wood by means of FT-IR and 2D IR correlation spectroscopy. Int. J. Biol. Macromol. 48, 667–675.

Popescu, M.C., Popescu, C.M., Lisa, G., Sakata, Y., 2011b. Evaluation of morphological and chemical aspects of different wood species by spectroscopy and thermal methods. J. Mol. Struct. 988, 65–72.

Popescu, C.M., Gradinariu, P., Popescu, M.C., 2016. Structural analysis of lime wood biodegraded by white rot fungi through infrared and two dimensional correlation spectroscopy. J. Mol. Struct. 1124, 78–84.

Proniewicz, L.M., Paluszkiewicz, C., Wesutecha-Birczynska, A., Majercherczyk, H., Baranski, A., Koniecczna, A., 2001. FT-IR and FT-Raman study of hydrothermally degraded cellulose. J. Mol. Struct. 596, 163–169.

Rahman, M.R., Hamdan, S., Lai, J.C.H., Jawaid, M., Bin Md Yusof, F.A., 2017. Physico-mechanical, thermal and morphological properties of furfuryl alcohol/2-ethylhexyl methacrylate/halloysite nanoclay wood polymer nanocomposites (WPNCs). Heliyon 3, e00342.

Sanjay, M.R., Madhu, P., Jawaid, M., Senthamaraikannan, P., Senthil, S., Pradeep, S., 2018. Characterization and properties of natural fiber polymer composites: a comprehensive review. J. Clean. Prod. 172, 566–581.

Santos, S.M., Carbajo, J.M., Quintana, E., Ibarra, D., Gomez, N., Ladero, M., Eugenio, M.E., Villar, J.C., 2015. Characterization of purified bacterial cellulose focused on its use on paper restoration. Carbohydr. Polym. 116, 173–181.

Sassi, J.-F., Tekely, P., Chanzy, H., 2000. Relative susceptibility of the I_α and I_β phases of cellulose towards acetylation. Cellulose 7, 119–132.

Schwanninger, M., Rodrigues, J.C., Pereira, H., Hinterstoisser, B., 2004. Structural analysis of photodegraded lime wood by means of FT-IR and 2D IR correlation spectroscopy. Vib. Spectrosc. 36, 23–40.

Segal, L., Creely, J.J., Martin, A.E., Conrad, C.M., 1959. An empirical method for estimating the degree of crystallinity of native cellulose using the X-ray diffractometer. Text. Res. J. 29, 786–794.

Shimur, R., Nishiok, A., Kano, I., Koda, T., Nishio, T., 2014. Novel method for producing amorphous cellulose only by milling. Carbohydr. Polym. 102, 645–648.

Song, Y., Zhang, J., Zhang, X., Tan, T., 2015. The correlation between cellulose allomorphs (I and II) and conversion after removal of hemicellulose and lignin of lignocellulose. Bioresour. Technol. 193, 164–170.

Stark, N.M., Matuana, L.M., 2004. Surface chemistry changes of weathered HDPE/wood-flour composites studied by XPS and FTIR spectroscopy. Polym. Degrad. Stab. 86, 1–9.

Sugiyama, J., Persson, J., Chanzy, H., 1991. Combined Infrared and Electron diffraction study of polymorphism of native cellulose. Macromolecules 24, 61–66.

Sun, X.F., Sun, R.C., Fowler, P., Baird, M.S., 2004. Isolation and characterisation of cellulose obtained by a two-stage treatment with organosolv and cyanamide activated hydrogen peroxide from wheat straw. Carbohydr. Polym. 55, 379–391.

Tamburini, D., Lucejko, J.J., Zoborowska, M., Modugno, F., Pradzynski, W., Colombini, M.P., 2015. Archaeological wood degradation at the site of Biskupin (Poland): wet chemical analysis and evaluation of specific Py-GC/MS profiles. J. Anal. Appl. Pyrolysis 115, 7–15.

Temiz, A., Yildiz, U.C., Aydin, I., Eikenes, M., Alfredsen, G., Olakoglu, G.C., 2005. Surface roughness and color characteristics of wood treated with preservatives after accelerated weathering test. Appl. Surf. Sci. 250, 35–42.

Watanabe, A., Morita, S., Ozaki, Y., 2006. Study on temperature-dependent changes in hydrogen bonds in cellulose I by infrared spectroscopy with perturbation-correlation moving-window two-dimensional correlation spectroscopy. Biomacromolecules 7, 3164–3170.

Zghari, B., Doumenq, P., Romane, A., Boukir, A., 2017. GC-MS, FTIR and ^{1}H, ^{13}C NMR structural analysis and identification of phenolic compounds in olive mill wastewater extracted from oued Oussefrou effluent (Beni Mellal-Morocco). J. Mater. Environ. Sci. 8, 4496–4509.

Zghari, B., Hajji, L., Boukir, A., 2018. Effect of moist and dry heat weathering conditions on cellulose degradation of historical manuscripts exposed to accelerated ageing: ^{13}C NMR and FTIR spectroscopy as a non-invasive monitoring approach. J. Mater. Environ. Sci. 9, 641–654.

Zhicheng, J., Jian, Y., Jianmei, L., Ting, H., Changwei, H., 2015. Promoting effect of sodium chloride on the solubilization and depolymerization of cellulose from raw biomass materials in water. ChemSusChem 8, 1901–1907.